Steering Edge Currents through a Floquet-Topological Insulator

Helena Drüeke[1] and Dieter Bauer[2]

Institute of Physics, University of Rostock, 18051 Rostock, Germany

Periodic driving may cause topologically protected, chiral transport along edges of a 2D lattice that, without driving, would be topologically trivial. We study what happens if one adds a different on-site potential along the diagonal of such a 2D grid. In addition to the usual bulk and edge states, the system then also exhibits doublon states, analogous to two interacting particles in one dimension. A particle initially located at an edge propagates along the system's boundary. Its wavefunction splits when it hits the diagonal and continues propagating simultaneously along the edge and the diagonal. The strength of the diagonal potential determines the ratio between both parts. We show that for specific values of the diagonal potential, hopping onto the diagonal is prohibited so that the system effectively separates into two triangular lattices. For other values of the diagonal potential, we find a temporal delay between the two contributions traveling around and through the system. This behavior could enable the steering of topologically protected transport of light along the edges and through the bulk of laser-inscribed photonic waveguide arrays.

I. INTRODUCTION

In the quantum Hall effect, a perpendicular magnetic field leads to circular currents of the electrons in a 2D material. The currents cancel within the bulk of the material, making it an insulator there. However, electrons may skip along edges, rendering the system a conductor at the surface. Topological insulators [1] are materials that exhibit an insulating bulk and conducting edges without an external magnetic field. In his Nobel-prizeawarded publication [2], Haldane proposed a model for a topological insulator on a hexagonal lattice by introducing complex next-nearest neighbor hopping. It was later found to exist similarly in real materials owing to spin-orbit coupling (see, e.g., [3] for a recent review).

Floquet-topological insulators are synthetic systems, which behave as topological insulators due to periodic driving [4]. Such synthetic systems are realized with cold atoms in optical lattices [5, 6] or with photonic platforms [7–11], for example.

Rudner *et al.* [12] proposed a Floquet-topological insulator and derived its proper topological invariants. In this publication, we investigate a modified version of that system where, instead of alternating on-site potentials on the two sublattices, we introduce increased onsite potentials along the diagonal of the lattice. The motivation to do so originated from doublon physics. There, two interacting particles on, for example, a onedimensional [13–16] or two-dimensional [17] lattice may form a bound pair, a doublon state. Doublons are stable due to their

energetic separation from other states or because of topology, characterized by a differing topological invariant. They can arise for repulsively as well as for attractively interacting particles.
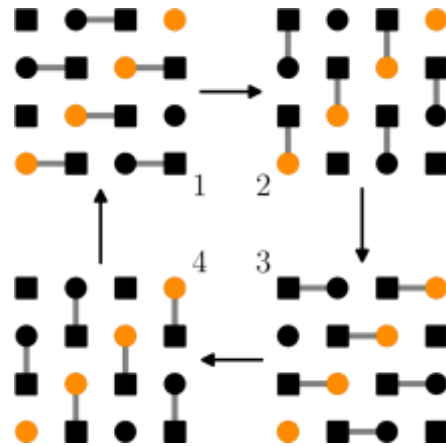
II. SYSTEM

FIG. 1. Sketch of the driving scheme for a 4×4 system. The dots (squares) indicate the lattice sites on sublattice A (B). The yellow dots are the lattice sites on the diagonal (with a modified on-site potential). The four panels show the different hoppings in the four phases of the driving cycle as gray connecting lines.

---

[1] helena.drueeke@uni-rostock.de

[2] dieter.bauer@uni-rostock.de

We investigate an $N \times N$ square-lattice system. The lattice sites $s_{i,j}$ are numbered by horizontal and vertical indices $i,j \in \{1,2,...,N\}$. The driving scheme determines two sublattices. Sublattice A contains all sites with even sum $i + j$, sublattice B those with odd $i + j$.

Previous studies [12] used global on-site potentials, such as alternating potentials on the two sublattices (e.g., positive on sublattice A, negative on sublattice B). These potentials affect all unit cells. We do not employ such global on-site potentials, but modify the potentials of the sites $s_{i,i}$ along the diagonal (as shown in Fig. 1), which we set to V_{dia}. All other on-site potentials remain 0.

The hoppings and local elements are described by the stepwise constant Hamiltonian

$$\hat{H}_k = \hat{H}_{\mathrm{dia}} + J \sum_{=1}^{N} \hat{h}_k(i,j) + \mathrm{h.c.},$$ (1)

$$\hat{H}(t) = \begin{cases} \hat{H}_1 & 0 < t \le T/4 \\ \hat{H}_2 & T/4 < t \le T/2 \\ \hat{H}_3 & \\ \hat{H}_4 & T/2 < t \le 3T/4 \end{cases}$$

with $\qquad\qquad\qquad\qquad\quad 3T/4 < t \le T$ (2)

$$\sum_{i,j}^{i+j \text{ even}}$$

$$N \hat{H}_{\mathrm{dia}} = V_{\mathrm{dia}}$$

$$\mathrm{X}_{|i,i\rangle\langle i,i|},$$ (3)

$$\sum_{i=1}$$

$$\hat{h}_1(i,j) = |i,j\rangle\langle i+1,j|, \quad \hat{h}_2(i,j) = |i,j\rangle\langle i,j+1|,$$
$$\hat{h}_3(i,j) = |i,j\rangle\langle i-1,j|, \quad \hat{h}_4(i,j) = |i,j\rangle\langle i,j-1|.$$ (4)

We set $J = 1$ and choose the timing of all four phases such that in the absence of on-site potentials the transfer probability between two connected sites during one phase is exactly one, i.e., $JT/4 = \pi/2$. With onsite potential V_{dia} along the diagonal, the transfer probability between diagonal and off-diagonal sites (and vice-versa) is given by

$$p(V_{\mathrm{dia}}) = \frac{4}{V_{\mathrm{dia}}^2 + 4} \sin^2\left(\frac{\pi}{4}\sqrt{V_{\mathrm{dia}}^2 + 4}\right),$$ (5)

derived in appendix A. The zeros of this equation are at

$$V_{\mathrm{dia},0}^{(n)} = \pm 2\sqrt{4n^2 - 1}$$ (6)

for $n \in \mathbb{N}$. We see that hopping onto the diagonal can be suppressed entirely (and the square lattice thus splits into two triangles) at a remarkably low diagonal potential $V_{\mathrm{dia},0}^{(1)} = 2\sqrt{3}.$

III.   METHODS

The time evolution operator (in units where $\sim = 1$)

$$\hat{U}(t) = \mathcal{T} \exp\left(-\mathrm{i} \int_0^t \mathrm{d}t' \, \hat{H}(t')\right),$$ (7)

where $\mathcal{T}$ is the time-ordering operator, describes the temporal evolution of the system. For a complete driving cycle $t = T$ consisting of the four discrete phases, the time evolution operator reads

$$\hat{U}(T) = e^{cH_4}e^{cH_3}e^{cH_2}e^{cH_1},$$ (8)

with $c = \frac{T}{4}\mathrm{i}$. Solving the equation

$$\hat{U}(T)\psi_F = \lambda_F \psi_F$$ (9)

gives the Floquet eigenstates ψ_F, and the Floquet energies ε_F are calculated from the eigenvalues $\lambda_F = \exp(-\mathrm{i}\varepsilon_F T)$. By following the states (not just their energies) as a function of V_{dia}, we can distinguish state crossings from avoided crossings. Appendix B explains the details of the state-tracking algorithm.
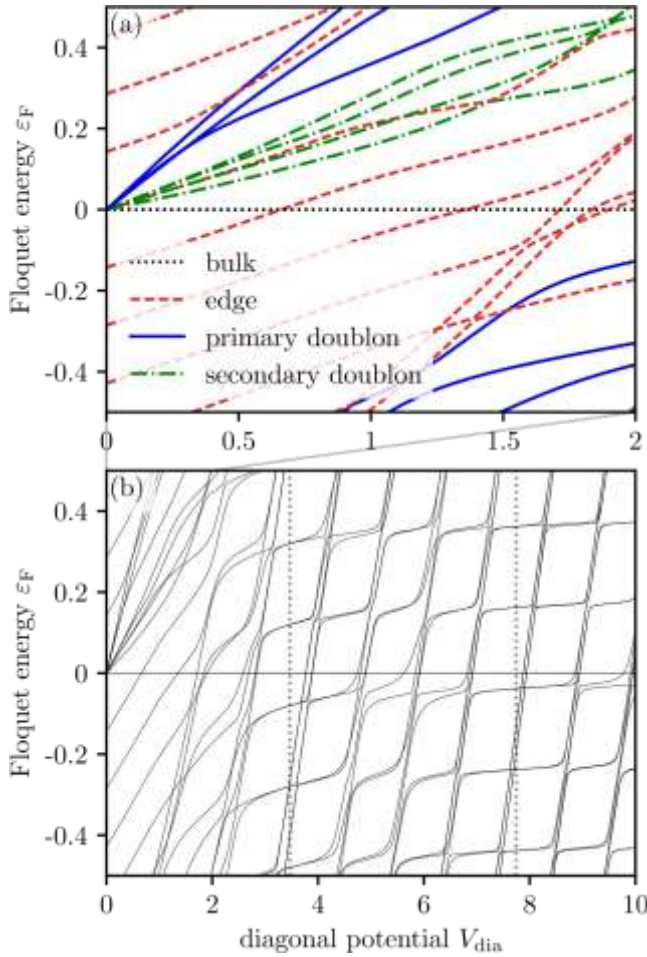
IV. FLOQUET STATES

FIG. 2. Floquet energies ε_F for the 4×4 system as a function of the diagonal potential V_{dia}. a) The line colors and styles indicate the types of states. b) The dotted gray lines indicate the zeros $V_{dia,0}^{(1)}$, $V_{dia,0}^{(3)}$ of the transfer probability $p(V_{dia})$.

Without a diagonal potential, the $N \times N$ system contains $(N-1)^2$ bulk states at Floquet energy $\varepsilon_F = 0$ and $2N-1$ edge states at equally spaced Floquet energies $\varepsilon_F = m/(2N-1)$, $m \in \mathbb{Z}$, $|m| < N$. At non-vanishing diagonal potential, some of the bulk states superpose to form diagonal states, resulting in $(N-3)(N-2)$ remaining bulk states, $N-1$ primary diagonal states, and $2(N-2)$ secondary diagonal states. Particles in a primary diagonal state hop on and off the modified diagonal twice during a complete driving cycle. They hop on and off the diagonal once in a secondary diagonal state.

We call these diagonal states *doublons*, in analogy to doublons in one-dimensional, interacting systems [13–17]. A system of two interacting particles on a onedimensional lattice (e.g., an SSH chain [18]) can be mapped to a single particle on a two-dimensional lattice. The x- and y-coordinates of the 2D particle correspond to the position of the first and the second particle on the 1D chain, respectively. Movements of the first (second) particle then amount to horizontal (vertical) hoppings. Their interaction $V(|x-y|)$ is captured by an on-site potential in 2D. A local interaction in 1D, through which the particles only affect each other if they are on the same site, corresponds to the diagonal potential along $x = y$ used in this study. Longer-range interactions would require non-vanishing on-site potentials on not only the main but also the secondary, tertiary, etc. diagonal, depending on the maximum interaction distance.

Figure 2 shows the Floquet energies ε_F as a function of the diagonal potential V_{dia}. The four different types of states are indicated in Fig. 2a: The diagonal potential does not influence the bulk states' energies because the bulk states remain located on sites whose potentials are zero in each step of the driving cycle. The edge states cross the diagonal in the system's bottom left and top right corners. Therefore, their energies increase with increasing diagonal potential. The doublons cross the diagonal as well, which leads to increasing Floquet energies. The primary doublons' energies increase faster because they cross the diagonal twice during a driving cycle, unlike the secondary doublons, which only cross it once.

At higher diagonal potentials $V_{dia} \gtrsim 2$ (shown in Fig. 2b), three types of states exist: The bulk states' energies remain zero, while the edge states' energies increase slightly with diagonal potential. For the Floquet states located on the diagonal of the system, we find $\varepsilon_F \approx V_{dia}$. All states form pairs with similar energies. At the zeros of the transfer probability, these pairs degenerate, and we find superpositions of the states which are confined to either the top left or bottom right triangular half of the system.

V. TEMPORAL EVOLUTION

By definition, the Floquet states ψ_F remain unchanged after a complete cycle's evolution, except for a phase factor. However, for an intuitive understanding of the driven quantum dynamics, it is instructive (and closer to experimental realizations on photonic platforms) to study the temporal evolution of (initially) localized states $\phi(\vec{r},t)$. We initialize these as one at a single site $\vec{r}_{initial}$ and zero everywhere else. Specifically, in Fig. 3, we look at the state starting in the top left corner of the 4 × 4 system.

Without a diagonal potential and therefore perfect transfer $p(0) = 1$ between diagonal and off-diagonal sites (Fig. 3a), the state remains localized and moves counter-
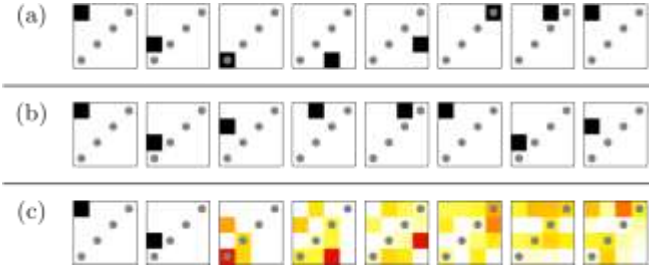
FIG. 3. Temporal evolution (snapshots after 0,1,...,7 complete driving cycles) of a localized state in a 4 × 4 system. a) $V_{dia} = 0$, i.e. $p(V_{dia}) = 1$, the state moves around the whole√ system and returns after $2N - 1 = 7$ cycles. b) $V_{dia} = 2\sqrt{3}$, i.e. $p(V_{dia}) = 0$, the state moves around the upper left triangle because the diagonal is insurmountable and returns after $2N - 3 = 5$ cycles. c) $V_{dia} = 1.59737$, i.e. $p(V_{dia}) = 0.5$, the state splits. The supplementary material contains animations of these three cases for a 10 × 10 system.

clockwise along the edges of the system, and returns to its origin after $2N - 1$ complete driving cycles. At the zeros of the hopping probability $p(V_{dia}) = 0$, the state cannot cross the diagonal. Because it started above the diagonal, it will remain in the upper left triangular half of the system, moving along the edge of that triangle and returning to its origin after $2N - 3 = 5$ cycles (Fig. 3b). For all other potentials, which result in $0 < p(V_{dia}) < 1$, the state splits at the bottom left corner of the system and delocalizes (Fig. 3c).

Most $((N - 3)(N - 2))$ of the $(N - 1)^2$ bulk states do not interact with any sites on the diagonal, and therefore their evolution is unaffected by V_{dia}. The other $3N - 5$ bulk states, however, interact with the diagonal at least once and are split up for $0 < p(V_{dia}) < 1$. For $p(V_{dia}) = 0$, $2N - 3$ bulk states turn into edge states on the upper left and lower right triangles. The $N - 2$ bulk and 2 edge states which start on the diagonal remain stationary for $p(V_{dia}) = 0$.

While snapshots of the temporal evolution allow us to understand the general behavior, it is not easy to investigate them systematically for varying potentials. Therefore, we record the probability density $|\phi(\sim r_{initial}, nT)|^2$ ($n \in \mathbb{N}$) at the starting location $\sim r_{initial}$ after each driving cycle. Because we initialize all states perfectly localized, $|\phi(\sim r_{initial}, 0)|^2 = 1$ for all states. The bulk states return to their starting location after each cycle and therefore $|\phi_{bulk}(\sim r_{initial}, nT)|_2 = 1 \; \forall n \in \mathbb{N}$.

As shown in Fig. 4, without a diagonal potential, an edge state returns back at its origin after $2N - 1$ cycles. At the zeros of $p(V_{dia})$ (6), the system is equivalent to one without

sites on the diagonal. There, the edge states remain confined to the upper left or bottom right triangle, which they started in, and return to their origins after $2N - 3$ cycles. Other on-site potentials V_{dia} lead to a splitting of the state. Part of the wavefunction travels through the diagonal and along the square's edge, arriving after $2N - 1$ cycles, while another part travels around the triangle and arrives after $2N - 3$ cycles. Due
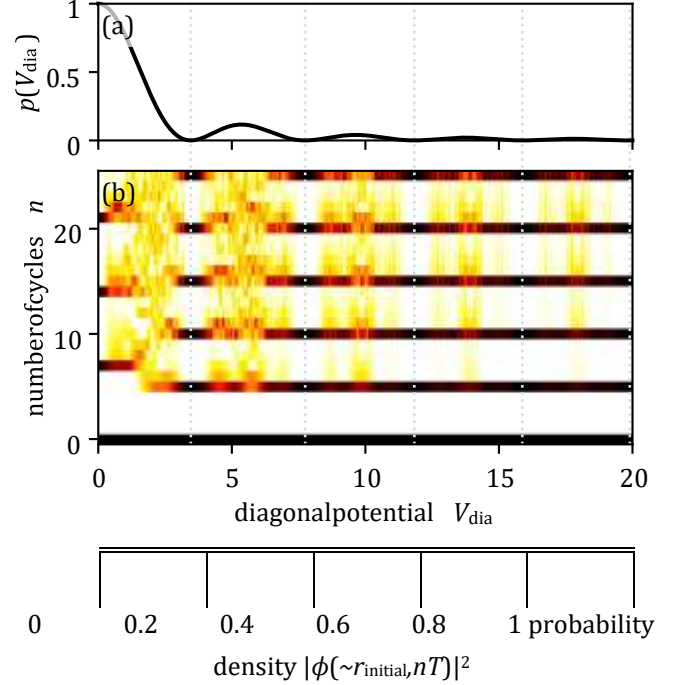

FIG. 4. a) Hopping probability $p(V_{dia})$ as a function of diagonal potential. b) Probability density $|\phi(\sim r_{initial}, nT)|^2$ ($n \in \mathbb{N}$) at the starting location $\sim r_{initial}$ for an edge state, as a function of time and diagonal potential. The dotted gray lines indicate the zeros of $p(V_{dia})$ in a), which coincide with the perfect earlier returns in b).

to the imperfect transfer, there are not two discrete arrival peaks. Instead, the peaks disperse and interfere.

VI.   CONCLUSION AND OUTLOOK

We characterized a Floquet-topological insulator on a square lattice with varying diagonal on-site potential. The addition of a diagonal potential causes the appearance of two additional bands. These bands consist of states that cross the square system's diagonal (once or twice during a driving cycle). We call these states doublons, in analogy

to doublons in systems of one-dimensional, interacting particles.

We showed how fine-tuning the diagonal potential allows switching between the propagation along the edge and propagation along the diagonal. In a photonic setting with laser-inscribed waveguides, intense laser light and nonlinearities can modify the diagonal potential (i.e., refractive index) [19]. In that way, one may switch topologically protected light currents by light, rendering a photonic platform programmable instead of "hardwired."

ACKNOWLEDGMENT

Appendix A: Derivation of hopping probability

The 2 × 2 Hamiltonian

$$\hat{H} = \begin{pmatrix} V & J \\ J & 0 \end{pmatrix} \tag{A1}$$

describes the hopping between two sites with potential difference V and hopping element J. Its eigenstates

$$\varphi_{1,2} = \begin{pmatrix} V \pm \sqrt{V^2 + 4J^2} \\ 2J \end{pmatrix} \tag{A2}$$

and corresponding eigenenergies

$$\varepsilon_{1,2} = \frac{1}{2}\left(V \pm \sqrt{V^2 + 4J^2}\right) \tag{A3}$$

satisfy the time-independent Schrödinger equation

$$\hat{H}\phi_{1,2} = \varepsilon_{1,2}\phi_{1,2}. \tag{A4}$$

The solutions of the time-dependent Schrödinger equation

$$\hat{H}\psi(t) = i\partial_t\psi(t) \tag{A5}$$

are superpositions of the eigenstates, $\psi(t) = a_1 \exp(-i\varepsilon_1 t)\phi_1 + a_2 \exp(-i\varepsilon_2 t)\phi_2.$ (A6)

For a time-dependent state starting localized on the first lattice site,

$$\begin{pmatrix} 1 \\ 0 \end{pmatrix} = \psi(0) = a_1\varphi_1 + a_2\varphi_2, \tag{A7}$$

we find

$$a_1 = -a_2 = \frac{1}{2\sqrt{V^2 + 4J^2}}. \tag{A8}$$

The transfer probability is the absolute square of the time-dependent state at the second lattice site,

$$p(t, V) = |\psi_2(t)|^2 \tag{A9}$$

$$= \frac{4J^2}{V^2 + 4J^2}\sin^2\left(\frac{\sqrt{V^2 + 4J^2}}{2}t\right). \tag{A10}$$

The driving period

$$T = \frac{2\pi}{J} \tag{A11}$$

is chosen such that, for $V = 0$, complete transfer happens during each of the four phases,

$$1 = p\left(\frac{T}{4}, 0\right). \tag{A12}$$

Finally, we find the hopping probability after a single phase of the driving cycle as a function of potential,

$$p(V) = p\left(\frac{T}{4}, V\right) \tag{A13}$$

$$= \frac{4J^2}{V^2 + 4J^2}\sin^2\left(\frac{\pi\sqrt{V^2 + 4J^2}}{4J}\right). \tag{A14}$$

Appendix B: Tracking States

We follow states through changing parameters, e.g. in the closed interval $[V_{dia,min}, V_{dia,max}]$. As a starting point, we calculate the Floquet energies $\varepsilon_{0,j}$ and states $\psi_{0,j}$ ($j = 1,2,...,N_xN_y$) at $V_0 = V_{dia,min}$. Then we loop through the following procedure: We increase the diagonal potential to $V_i = V_{i-1} + \delta$, with $0 < \delta \leq$ $V_{dia,max} - V_{dia,min}$, and calculate the new Floquet energies $\varepsilon_{i,k}$ and states $\psi_{i,k}$ ($k = 1,2,...,N_xN_y$). Each of the states $\psi_{i,k}$ is compared to all states $\psi_{i-1,j}$ from the previous step by calculating their overlap (scalar product).

The index l of the most similar previous state $\psi_{i-1,l}$ (with $|\psi_{i,k} \cdot \psi_{i-1,l}| \geq |\psi_{i,k} \cdot \psi_{i-1,j}| \; \forall j$) is stored in a similarity variable $s_{i,k} = l$.

If the mapping of states from the previous parameter V_{i-1} to the current parameter V_i is not bijektive, i.e. $s_{i,k} = s_{i,k_0}$ for $k \neq k_0$ (as shown in Fig. 5a), the states could not be followed because they have changed too much. In this case, δ must be decreased (in our calculations to $\delta_0 = \delta/10$), and the step repeated for $V_i = V_{i-1} + \delta_0$.

If the mapping was successful (Fig. 5b), δ may be kept constant or increased before the next step to V_{i+1}. We repeat these steps until we reach $V_{dia,max}$.

This adaptive-stepsize tracking works for non-zero diagonal potentials but breaks down at $V_{dia} = 0$, where the doublon states all collapse to localized bulk states at $\varepsilon_F = 0$ and can not be followed.

[1] M. Z. Hasan and C. L. Kane, Colloquium: Topological insulators, Reviews of Modern Physics **82**, 3045 (2010).

[2] F. D. M. Haldane, Model for a Quantum Hall Effect without Landau Levels: Condensed-Matter Realization of the "Parity Anomaly", Physical Review Letters **61**, 2015 (1988).

[3] M. Nadeem, A. R. Hamilton, M. S. Fuhrer, and X. Wang, Quantum Anomalous Hall Effect in Magnetic Doped Topological Insulators and Ferromagnetic SpinGapless Semiconductors—A Perspective Review, Small **16**, 1904322 (2020).

[4] N. H. Lindner, G. Refael, and V. Galitski, Floquet topological insulator in semiconductor quantum wells, Nature Physics **7**, 490 (2011).

[5] G. Jotzu, M. Messer, R. Desbuquois, M. Lebrat, T. Uehlinger, D. Greif, and T. Esslinger, Experimental realization of the topological Haldane model with ultracold fermions, Nature **515**, 237 (2014).

[6] K. Wintersperger, C. Braun, F. N. Ünal, A. Eckardt, M. D. Liberto, N. Goldman, I. Bloch, and M. Aidelsburger, Realization of an anomalous Floquet topological system with ultracold atoms, Nature Physics **16**, 1058 (2020).

[7] M. C. Rechtsman, J. M. Zeuner, Y. Plotnik, Y. Lumer, D. Podolsky, F. Dreisow, S. Nolte, M. Segev, and A. Szameit, Photonic Floquet topological insulators, Nature **496**, 196 EP (2013).

[8] M. Segev and M. A. Bandres, Topological photonics: Where do we go from here?, Nanophotonics **10**, 425 (2021).

[9] M. Hafezi, S. Mittal, J. Fan, A. Migdall, and J. M. Taylor, Imaging topological edge states in silicon photonics, Nature Photonics **7**, 1001 (2013).

[10] M. S. Kirsch, Y. Zhang, M. Kremer, L. J. Maczewsky, S. K. Ivanov, Y. V. Kartashov, L. Torner, D. Bauer, A. Szameit, and M. Heinrich, Nonlinear second-order photonic topological insulators, Nature Physics **17**, 995 (2021).

[11] S. K. Ivanov, Y. V. Kartashov, M. Heinrich, A. Szameit, L. Torner, and V. V. Konotop, Topological dipole Floquet solitons, Physical Review A **103**, 053507 (2021).

[12] M. S. Rudner, N. H. Lindner, E. Berg, and M. Levin, Anomalous Edge States and the Bulk-Edge Correspondence for Periodically Driven Two-Dimensional Systems, Physical Review X **3**, 031005 (2013).

[13] M. Valiente, Lattice two-body problem with arbitrary finite-range interactions, Physical Review A **81**, 042102 (2010).

[14] M. Di Liberto, A. Recati, I. Carusotto, and C. Menotti, Two-body physics in the Su-Schrieffer-Heeger model, Physical Review A **94**, 062704 (2016).

[15] A. M. Marques and R. G. Dias, Topological bound states in interacting Su–Schrieffer–Heeger rings, Journal of Physics: Condensed Matter **30**, 305601 (2018).

[16] P. M. Azcona and C. A. Downing, Doublons, topology and interactions in a one-dimensional lattice, Scientific Reports **11**, 12540 (2021).

[17] G. Salerno, G. Palumbo, N. Goldman, and M. Di Liberto, Interaction-induced lattices for bound states: Designing flat bands, quantized pumps, and higher-order topological insulators for doublons, Physical Review Research **2**, 013348 (2020).

[18] W. P. Su, J. R. Schrieffer, and A. J. Heeger, Solitons in Polyacetylene, Physical Review Letters **42**, 1698 (1979).

[19] L. J. Maczewsky, M. Heinrich, M. Kremer, S. K. Ivanov, M. Ehrhardt, F. Martinez, Y. V. Kartashov, V. V. Konotop, L. Torner, D. Bauer, and A. Szameit, Nonlinearityinduced photonic topological insulator, Science **370**, 701 (2020).
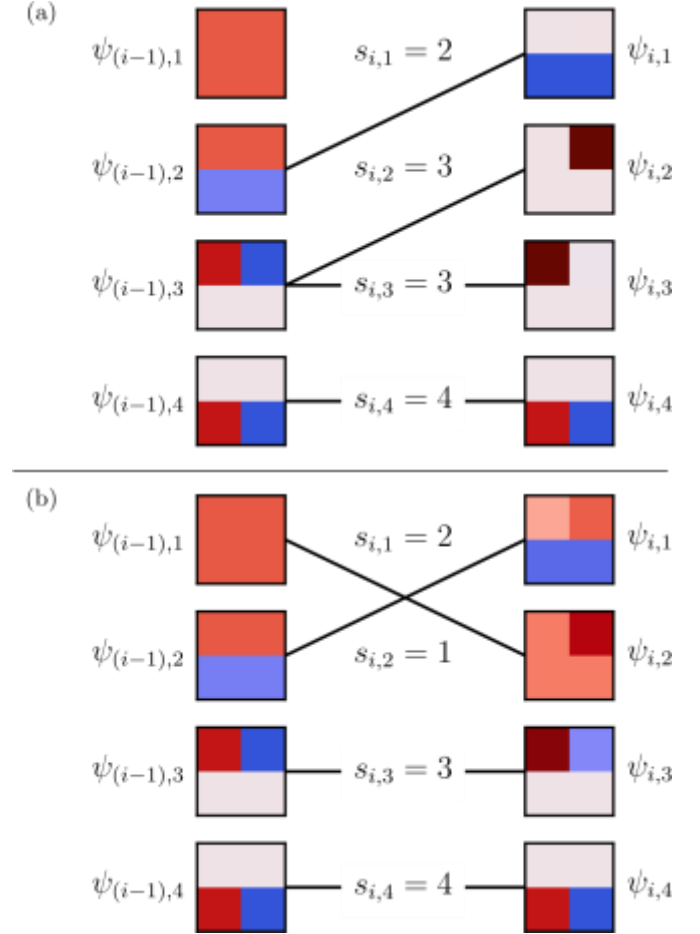
FIG. 5. a) Example of tracking algorithm failure. Both $\psi_{i,2}$ and $\psi_{i,3}$ are most similar to (i.e. have the largest overlap with) the same state $\psi_{(i-1),3}$ from the previous step ($s_{i,2} = s_{i,3} = 3$). We can not track the evolution of $\psi_{(i-1),3}$ unambiguously. Therefore, we must repeat the step from $i − 1$ to i using a smaller step size. b) Example of tracking algorithm success. The states $\psi_{(i-1),j}$ map biuniquely to the states $\psi_{i,k}$ ($j,k = 1,2,3,4$).